

Rhodamine 6g Removal from Aqueous Solution with Coconut Shell-Derived Nanomagnetic Adsorbent Composite (Cs-Nmac): Isotherm and Kinetic Studies

Palsan Sannasi Abdullah*, Lim Kai Wen, Huda Awang and Siti Nuurul Huda Mohammad Azmin

Faculty of Agro-Based Industry, Universiti Malaysia Kelantan, Jeli Campus 17600 Jeli, Kelantan, Malaysia

ABSTRACT

Untreated effluents from the textile industry containing colorant dyes are harmful to the environment, aquatic organisms, and human health. Among these effluents, Rhodamine 6G is known as a corrosive and irritant dye. A coconut shell-derived nanomagnetic adsorbent composite (CS-NMAC) was developed to remove Rhodamine 6G from aqueous solution. Physical and adsorption properties of CS-NMAC were characterized via Brunauer–Emmett–Teller (BET) surface area analysis (S_{BET} : 1092.17 m²/g; total pore volume: 0.6715 cm³/g), X-ray diffraction (Fe₃O₄ [θ =35.522], Fe₂O₃ [θ =35.720] and FeO [θ =41.724]) and Fourier transform infrared spectroscopy (Fe–O, C–H, asymmetric C=C=C, CN and O–H). CS-NMAC was found to be electropositive within a broad pH range of 3–10) owing to the presence of nanoscale iron oxides on the surface of the coconut shell-derived adsorbent that enhanced the chemical and electrochemical outputs. Isotherm study revealed that the adsorption process of Rhodamine 6G followed a multilayer type of adsorption onto a heterogeneous surface. Freundlich model fitted better ($R^2 = 0.981$) than

the other models (Langmuir, Temkin and BET). The maximum adsorption capacity was 32.02 mg/g. Rhodamine 6G removal by CS-NMAC obeyed the pseudo-second-order reaction ($R^2 = 0.9995$) as opposed to other kinetic models. CS-NMAC has the potential to become an effective treatment for dye pollution.

ARTICLE INFO

Article history:

Received: 10 February 2021

Accepted: 21 May 2021

Published: 31 July 2021

DOI: <https://doi.org/10.47836/pjst.29.3.40>

E-mail addresses:

palsan.abdullah@umk.edu.my (Palsan Sannasi Abdullah)

kaiwenlim1@gmail.com (Lim Kai Wen)

hudaawang@gmail.com (Huda Awang)

huda.ma@umk.edu.my (Siti Nuurul Huda Mohammad Azmin)

*Corresponding author

Keywords: Adsorption, dye, isotherm, nanomagnetic, Rhodamine 6G

INTRODUCTION

Textile operators are the 3rd largest exporter of Malaysian products and a notable contributor to the country's economic growth (Azlan & Haseeb, 2019). However, the industry consumes enormous amounts of water and dyes during manufacturing processes. The effluents containing dyes derived from the textile industry continuously contaminate the water resources (Sundarajoo & Maniyam, 2019).

Rhodamine 6G is an azo dye with one or more $-N=N-$ groups attached to an aromatic structure. The dye is chemically stable and recalcitrant because of its chromophoric characteristics (Miranda et al., 2019).

Exposure to Rhodamine 6G dye is detrimental to health as it can cause allergic dermatitis and severe damage to the nervous system (Rasheed & Bilal, 2017). Over the past decades, many approaches for cleaning up dye pollutants have been developed and applied (Sahu & Singh, 2019). According to Wimalawansa (2013), the commonly used water treatment methods are chemical coagulation, sludge sedimentation, filtration, reverse osmosis, and carbon adsorption. Among these methods, activated carbon is widely used in the industry to remove dye pollutants. Although activated carbon is effective for cleaning up dye pollutants, its cost can become high (Sahu & Singh, 2019). Several approaches that involve the use of adsorbents have been proposed to overcome this problem. For example, *Clitoria fairchildiana* pods can adsorb up to 73.84 mg g^{-1} of Rhodamine 6G dye through chemisorption, but its application is time consuming (Miranda et al., 2019). Ni–Al-layered double oxides can remove dyes with 16% removal efficiency (Intachai et al., 2019). Therefore, high-quality adsorbents must not only be cost effective but also have competitive performance and are environmentally friendly (Suwunwong et al., 2020).

Various biocarbon materials have attracted increased attention owing to their innovativeness, modifiability, low cost, ease of preparation and ecofriendliness. Biocarbon is a carbon-rich, porous, and finely ground materials derived from carbonaceous biomass through limited air thermal decomposition process (Godwin et al., 2019). The biocarbon surface is generally negatively charged because of the dissociation of functional groups containing oxygen. As biocarbon uses carbonaceous biomass for processing, agricultural wastes can be possibly exploited to produce biocarbon (Vyavahare et al., 2019). Coconut wastes have been identified as a potential carbonaceous biomass for biocarbon because of its abundance, high biodegradability, and low cost (Nadzri et al., 2020). Moreover, the ash of coconut shells contains silicon oxide (SiO_2) at the same level as the components of metal matrix composites (Bahrami et al., 2016). The International Union of Pure and Applied Chemistry classifies the pore diameter of coconut shell biocarbon (micropores) with mesoporosity having the average pore diameter of adsorbent pores (Muzarpar et al., 2020). Therefore, the biocarbon derived from coconut shells is a potent adsorbent (Nadzri et al., 2020).

Although the performance of biocarbon in removing pollutants is effective, the separation of powdered biocarbon from an aqueous solution is difficult (Godwin et al., 2019). Physical modifications have been made to overcome this problem. Magnetic precursors, such as hematite, magnetite, siderite, and pyrite, are transformed into magnetic particles and attached onto the biocarbon surface. The application of magnetic particles to the separation process has been getting attention since the 1990s (Booker et al., 1991). Magnetic properties facilitate the separation of biocarbon from aqueous solution, thereby avoiding secondary pollution (Feng et al., 2020). However, magnetic powdered carbon adsorbent aggregates with weak dispersion in the presence of a magnetic field; thus, the application of iron oxide nanoparticles to powdered activated carbon not only rapidly adsorbs contaminants but also has a stronger ferromagnetic property that can be homogeneously dispersed in solution (Guo et al., 2020).

Moreover, the synthesis of coconut shell-derived nanomagnetic adsorbent composites (CS-NMAC) involves chemical coprecipitation. In this study, chemical coprecipitation was adopted because this process is easy to control. The common magnetic precursors used in the chemical coprecipitation were Fe^{3+} and Fe^{2+} . A magnetic precipitate was generated on the surface of the adsorbent composite by adding an alkaline solution into the magnetic precursor solution with the dispersed adsorbent composites (Feng et al., 2021). Furthermore, a surfactant crosslinker was applied in the synthesis process to obtain relatively stable nanomagnetic adsorbent composites (Li et al., 2019).

Many studies have investigated the adsorption of Rhodamine 6G. However, the mechanism of adsorption by CS-NMAC has not been elucidated yet. CS-NMAC contains magnetite (FeO^-) that has an interesting property: it is an amphoteric compound. Therefore, the efficiency of dye removal using CS-NMAC was investigated in terms of isotherm, kinetics, and mechanisms during adsorption reaction.

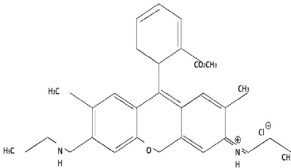
MATERIALS AND METHODS

Chemicals and Reagents

All chemicals and reagents used in this study, namely, ammonium hydroxide ($\text{NH}_3 \cdot \text{H}_2\text{O}$), ammonium hydroxide (NH_4OH), hydrochloric acid (HCl), nitric acid (HNO_3), sulfuric acid (H_2SO_4), sodium hydroxide (NaOH), potassium hydroxide (KOH), iron (III) chloride hexahydrate ($\text{FeCl}_3 \cdot 6\text{H}_2\text{O}$), iron (II) sulphate heptahydrate ($\text{FeSO}_4 \cdot 7\text{H}_2\text{O}$), potassium hydroxide (KOH), 70% of ethanol and distilled water, were of analytical grade. Commercial activated carbon (CAC) obtained from Friendemann Schmidt. Rhodamine 6G dye was purchased from Sigma Life Science. Rhodamine 6G, also known as basic red 1 ($\text{C}_{28}\text{H}_{31}\text{N}_2\text{O}_3\text{Cl}$), with 95% dye content was used without further purification. The properties of Rhodamine 6G are given in Table 1.

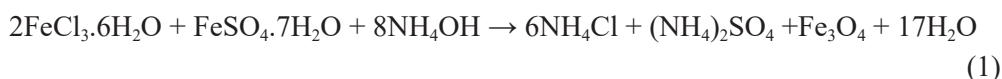
Table 1

Properties of Rhodamine 6G

Molecular name	Molecular formula	Molecular structure	Molecular weight (g mol ⁻¹)	Solubility (mg mL ⁻¹)	Colour
Rhodamine 6G	C ₂₈ H ₃₁ ClN ₂ O ₃		479.01	20	Red brown

Preparation of CS-NMAC

The preparation process commenced with carbonization of raw CS via the modified top lit up draft carbonization drum method. Afterward, the carbonized CS was ground into powder. CS-NMAC was prepared following a previously described method with slight modifications (Sannasi et al., 2021; Wannahari et al., 2018). The specific surface area and pore volume of the carbonized CS powder were increased by subjecting it to KOH activation at a ratio of 1:3 (carbonized CS powder:KOH) with slow agitation. The mixture was left for approximately 5–6 h to ensure complete intercalation of K into carbon compound. The intercalation reaction resulted in permanent expansion of carbon lattice in the carbon matrix (Wang & Kaskel, 2012). Subsequently, KOH was washed away from the expanded carbon lattice in the carbon matrix by repeatedly using deionized water (ddH₂O). The clean powder was dried at 90°C–100°C prior to heating at 800°C–900°C at a rate of 10°C/min for 15–30 min in a muffle furnace. The obtained sample allowed to cool down and then neutralized with 5% HCl before subsequent modification steps. CS-NMAC synthesis involved treatment with nitric acid (HNO₃) solution for 1 h at 80 °C to remove impurities from the adsorbent surface. A solution was then prepared with continuous stirring. First, FeCl₃.6H₂O and FeSO₄.7H₂O were dissolved in 450 mL of ddH₂O for 30 min at 30°C. Afterward, 30–60 mL of NH₄OH was added at 70°C for 1 h, followed by 5 g ammonium hydroxide (NH₃.H₂O) solution and the CS-modified biocarbon powder. Finally, 6 mL of epichlorohydrin was added into the solution and mixed at 85°C for 1 h. Epichlorohydrin served as a crosslinker to form chemical bonds between Fe₃O₄ and the CS-modified biocarbon powder. The solution was sonicated (Q Sonica) at 80 λ for 1 h, followed by more continuous stirring at 85°C for 1 h. The mixture that formed with precipitate allowed to cool down at 28°C, and the precipitate was washed with ddH₂O and ethanol. The sample (CS-NMAC) was dried at 50°C and collected using an external magnetic bar. The chemical reaction for generating CS-NMAC is as defined in Equations 1 and 2.



Sample Purification

The newly synthesized CS-NMAC was sorted according to particle size range by using a sieve filter (45–300 μm). The samples were repeatedly washed and filtered to remove impurities until the filter appeared clear with a pH approaching 7. The samples were dried in an oven at 80°C for 3–5 d and later kept in a container prior to use.

Characterization of CS-NMAC

Images of CAC and CS-NMAC were obtained using a scanning electron microscope (Jeol JSM-IT100) with a voltage of 10 KV at 2000 \times magnification. CS-NMAC morphology was examined via X-ray diffraction (XRD; Bruker, D8 Advance XRD) under following conditions: room temperature; CuK α radiation $\lambda=1.5406 \text{ \AA}$; and scan range $2\theta: 5^\circ\text{--}90^\circ$. The diffraction peaks were analysed using the Diffract Plus Eva software. CS-NMAC surface characteristics, including Brunauer–Emmett–Teller (BET) surface area, pore volume and pore size, were obtained via BET analysis of N₂ adsorption–desorption isotherm measurement at 77 K. Infrared spectrum of absorption was measured via Fourier transform infrared (FTIR) spectroscopy to identify chemical bonds. Functional groups and molecular components were detected and identified from the infrared absorption spectrum (Jasmin et al., 2013).

Effect of Contact Time and pH

The experiment was performed in batch mode under following parameters: room temperature (27 °C); 25.5 mg L⁻¹ initial dye concentration; 0.05 g CS-NMAC; and agitation at 150 rpm (Orbital shaker 14A-OBS602). The effects of contact time were evaluated by analysing the samples for 15–60 min and again for 5–30 min to determine the existence of quasiequilibrium situation according to patterns of adsorption at shorter times. The effects of pH were assessed by analysing the samples at pH 3–10.

Batch Adsorption Experiment

First, 0.05 g of CS-NMAC was added into Rhodamine 6G solution at different concentrations (1–15 mg/mL) and agitated at 150 rpm. Afterward, CS-NMAC was separated from the sample solution using an external magnetic bar. The remaining solution was analysed using a Thermo Scientific Genesys 20 UV–Visible spectrophotometer at 440–570 nm.

The adsorption capacity of Rhodamine 6G dye by CS-NMAC at equilibrium, q_e (mg/g), was determined by Equation 3.

$$q_e = \left[\frac{C_o - C_e}{W} \right] V, \quad (3)$$

where q_e is the amount of Rhodamine 6G dye adsorbed to the adsorbent (mg/g or mg g⁻¹), C_o is the initial concentration of Rhodamine 6G dye (mg L⁻¹), C_e is the equilibrium concentration of Rhodamine 6G dye (mg L⁻¹), V is the volume of solution (L) and W is the weight of adsorbents (CS-NMAC) used (g).

The percentage of Rhodamine 6G dye removal was calculated from Equation 4.

$$\% \text{ Adsorption or } \% \text{ Dye Removal} = \left[\frac{C_o - C_e}{C_o} \right] \times 100\% \quad (4)$$

Where C_o (mg L⁻¹) and C_e (mg L⁻¹) are the initial concentration and the equilibrium concentration of Rhodamine 6G dye, respectively.

Adsorption Isotherm and Kinetic Studies

Adsorption equilibrium experiments were conducted using different concentrations of Rhodamine 6G dye solution (5, 10, 15, 20, and 25 mg L⁻¹) under optimized parameters: contact time of 14.33 min, adsorbent dose of 0.05 g, particle size of 190.26 μm and pH 6.54. The equilibrium data calculated from the formula were used to fit the corresponding isotherm models. Freundlich, Langmuir and Temkin isotherms are widely adopted in dye removal studies (Santhi & Kumar, 2015; Wannahari et al., 2018). Variations in different isotherm models with their corresponding linear form of isotherm models are presented in Table 2. In the present study, Langmuir, Freundlich and Temkin isotherms were calculated using Equations 5, 6, and 7, respectively, to determine the adsorption capacity of the adsorbents at different concentrations of dye solution.

$$q_e = qm - \left(\frac{1}{KL} \right) \left(\frac{q_e}{C_e} \right) \quad (5)$$

Where q_e is the uptake of Rhodamine 6G at equilibrium (mg/g), qm is Langmuir maximum uptake of adsorbate per unit mass of adsorbent (mg/g), K_L is Langmuir constant related to rate of adsorption (L/mg) and C_e is concentration of Rhodamine 6G at equilibrium (mg/L) (Wannahari et al., 2018).

$$\ln q_e = \ln KF + \left(\frac{1}{n} \right) \ln C_e \quad (6)$$

Where q_e is the uptake of Rhodamine 6G at equilibrium (mg/g), K_F is the Freundlich adsorption constant (L/mg) and C_e is the concentration of Rhodamine 6G at equilibrium (Wannahari et al., 2018).

$$q_e = \left(\frac{RT}{b} \right) \ln Kt + \left(\frac{RT}{b} \right) \ln C_e \quad (7)$$

Where q_e is the uptake at equilibrium (mg/gb), b is Temkin constant (heat of sorption) (J/mol) and Kt is Temkin isotherm constant (Lg^{-1}) (Nimibofa et al., 2017).

The kinetics of Rhodamine 6G removal were investigated under optimized parameters of 26.12 mg/L dye concentration, 0.05 g adsorbent dose, 190.26 μm particle size and pH 6.54 and different contact times ranging from 5 min to 25 min with a time interval of 5 min. The kinetics of Rhodamine 6G adsorption from aqueous solution were analysed using pseudo-first-order, pseudo-second order and intra-particle diffusion models. The compatibility of the experimental data with the kinetic model was ensured using the correlation coefficient (R^2) value. A high R^2 value indicates that the model fits the Rhodamine 6G dye adsorption kinetics (Vijayakumar et al., 2012). The equations for pseudo-first-order, pseudo-second order and intra-particle diffusion kinetic models are given in Equation 8, 9, and 10, respectively.

$$\ln(q_e - qt) = \ln q_e - K_1 t \quad (8)$$

Where q_e is the amount of Rhodamine 6G adsorbed at equilibrium (mg/g), qt is the amount of dye adsorbed at any time (mg/g) and K_1 is a rate constant of the pseudo-first-order kinetic model (min^{-1}) (Vijayakumar et al., 2012).

$$\frac{t}{qt} = \frac{1}{K_2 q_e^2} + \frac{t}{q_e} \quad (9)$$

Where q_e is the uptake of Rhodamine 6G at equilibrium (mg/g), qt is the uptake of Rhodamine 6G at any time (mg/g) and K_2 is the rate constant for pseudo-second-order kinetic model (min^{-1}) (Vijayakumar et al., 2012).

$$q_t = k_i t^{\frac{1}{2}} + c \quad (10)$$

Where qt is the uptake of Rhodamine 6G at any time (mg/g), k_i is intra-particle diffusion rate constant ($\text{mg/g} \cdot \text{min}^{-1}$) and c is a constant of the thickness of the boundary layer (mg/g) (Wannahari et al., 2018).

Comparison between CS-NMAC and CAC in Rhodamine 6G removal

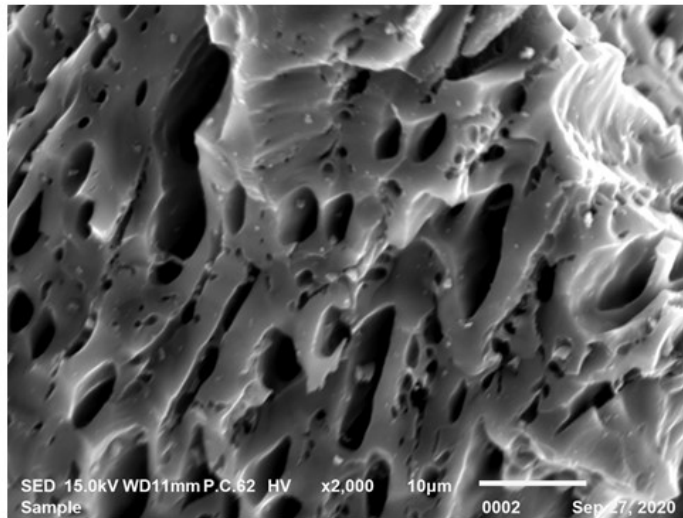
First, 0.05 g each of 74–250 μm CS-NMAC and CAC was added into an Erlenmeyer flask containing 26 mg/L Rhodamine 6G (pH 6.54). Afterward, the samples were agitated at 180 rpm for 14 min. The sample containing CS-NMAC was then separated using a magnet and a filter paper. Meanwhile, the sample containing CAC was filtered using a filter paper. Finally, the absorbance at 530 nm for each sample was recorded using a spectrophotometer.

RESULTS AND DISCUSSION

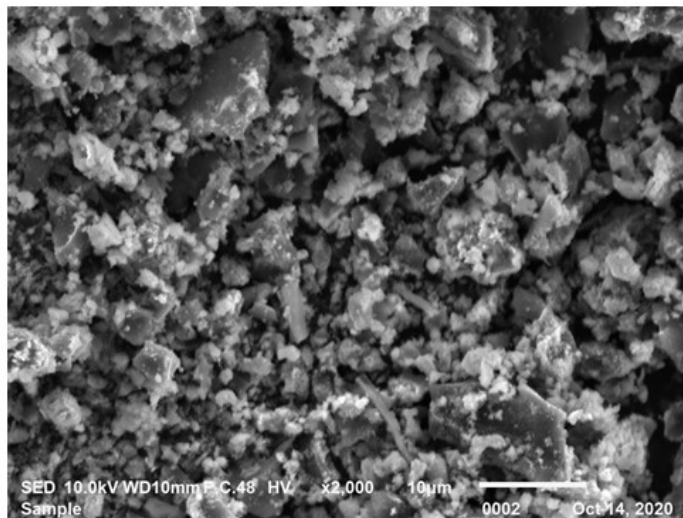
Characterization of CS-NMAC

The morphological structures of both CAC and CS-NMAC are presented in Figure 1.

Compared with CAC, iron oxide nanoparticles are embedded on the CS-NMAC matrix without obvious aggregations. This condition indicated that the CS-NMAC matrix and the iron oxide nanoparticles had a good mechanical binding.



(a)



(b)

Figure 1. SEM images of (a) CAC and (b) CS-NMAC at 2000× magnification at 10.0 kV

The surface of the CS-derived adsorbent was modified by adding iron oxide nanoparticles. The existence of these nanosized iron oxide materials on the surface of CS-NMAC was confirmed via XRD analysis (Figure 2). The iron oxide nanoparticles, namely, magnetite (Fe_3O_4), maghemite ($\gamma\text{-Fe}_2\text{O}_3$), hematite ($\alpha\text{-Fe}_2\text{O}_3$) and wuestite (FeO), are superparamagnetic; thus, they display a strong ferromagnetic behaviour (Kandpal et al., 2014).

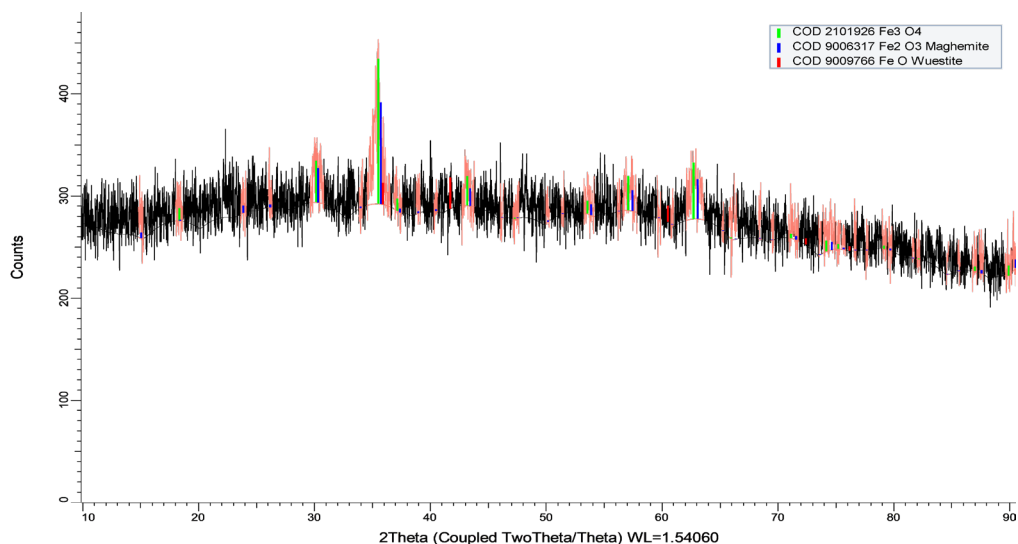


Figure 2. X-ray diffractogram for CS-NMAC with 100% relative intensity spectra for Fe_3O_4 ($\theta=35.522$), Fe_2O_3 ($\theta=35.720$) and FeO ($\theta=41.724$)

The BET surface area (S_{BET}) and total pore volume (TPV) of CS-NMAC were $1092.17 \text{ m}^2/\text{g}$ and $0.6715 \text{ cm}^3/\text{g}$, respectively. These S_{BET} and TPV values of CS-NMAC were higher than those of other magnetic adsorbents reported in the literature: -magnetic iron oxide nanoparticles derived from *Cyanometra ramiflora* fruit extract waste ($107.97 \text{ m}^2/\text{g}$, $0.13 \text{ cm}^3/\text{g}$) (Bishnoi et al., 2017); magnetic biochar derived from *Astragalus membranaceus* residues ($203.7 \text{ m}^2/\text{g}$, $0.187 \text{ cm}^3/\text{g}$) (Kong et al., 2017); activated carbon derived magnetic CS ($951.84 \text{ m}^2/\text{g}$, $0.6715 \text{ cm}^3/\text{g}$) (Hao et al., 2018); and magnetic corn waste straw ($313.9 \text{ m}^2/\text{g}$, $0.22 \text{ cm}^3/\text{g}$) (Khan et al., 2020). Thus, CS-NMAC is expected to have a better performance in adsorption than the magnetic iron oxide nanoparticles derived from other carbonaceous biomass owing to its high porosity.

Effects of Contact Time and pH

The effects of contact time on the percentage of Rhodamine 6G removal are depicted in Figure 3(a). The percentage of Rhodamine 6G removed was paltry after 33 min. Thus, steady state approximation was likely reached, and this result was accepted as a

quasiequilibrium situation (Mane & Babu, 2011). By contrast, at the second phase (after 33 min), the process became slow as repulsive forces occurred between the adsorbate and the adsorbent. The reaction achieved the maximum point when a longer contact time was applied.

The quasiequilibrium situation for a shorter time (below 30 min) was also tested in a separate experiment [Figure 3(b)]. The percentage of dye removed gradually increased from 5 min to 20 min, and the increase in the amount of dye removed was small from 20 min to 30 min. According to Patrick et al. (2014), at the initial phase of the adsorption process, adsorption rapidly occurs there are more vacant and available sites.

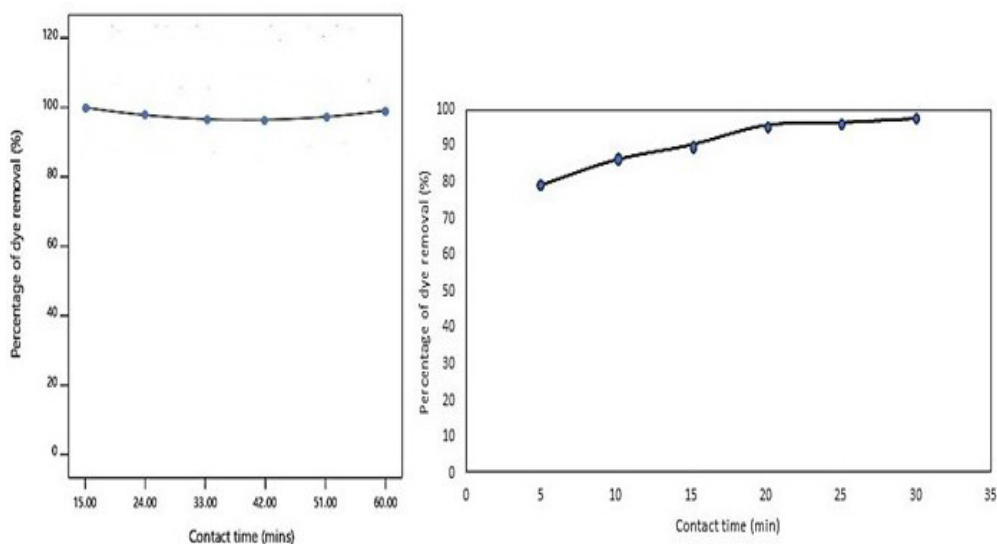


Figure 3. Percentage removal (%) of Rhodamine 6G by CS-NMAC in batch adsorption reaction at 27°C, 150 rpm and 0.05 g CS-NMAC according to (a) 15–60 min and (b) 5–30 min of contact time.

The initial solution pH was tested because pH governs the surface charge of CS-NMAC and speciation of polluting dyes. The percentage of dye removed increased as pH increased (Figure 4), demonstrating that CS-NMAC was electropositive within a wide range of pH from 3 to 10. The initial pH of the dye solution affected the functional groups on the surface of CS-NMAC. Adsorption occurred because of electrostatic interaction (alkene) and hydrogen bonding (hydroxyl) on the surface of CS-NMAC and the dye. According to Ahmadgurabi et al., (2018), the cationic functional group (NH^+) of Rhodamine 6G forms a hydrogen bond with the anionic functional (FeO^-) of CS-NMAC in basic pH media. Such reaction occurred because magnetite (FeO^-) has amphoteric properties. Moreover, the nature of CS-NMAC was electropositive within a wide pH range (3–10) during adsorption

because the alkaline mineral ash on the surface of the adsorbent was released into the solution (Kuang et al., 2020).

Furthermore, pH only had a slight effect on the percentage of dye removed not only because of the presence of amphoteric FeO^- functional group on the CS-NMAC surface but also because of the salting out effect phenomenon, which occurred because high salt concentrations affect pH and solution solubility. Decreases in the amount of Rhodamine 6G dye in solution due to the salting out effect induced the diffusion towards the hydrophobic surface of CS-NMAC. Such interaction later increased adsorption efficiency (Reguyal & Sarmah, 2018).

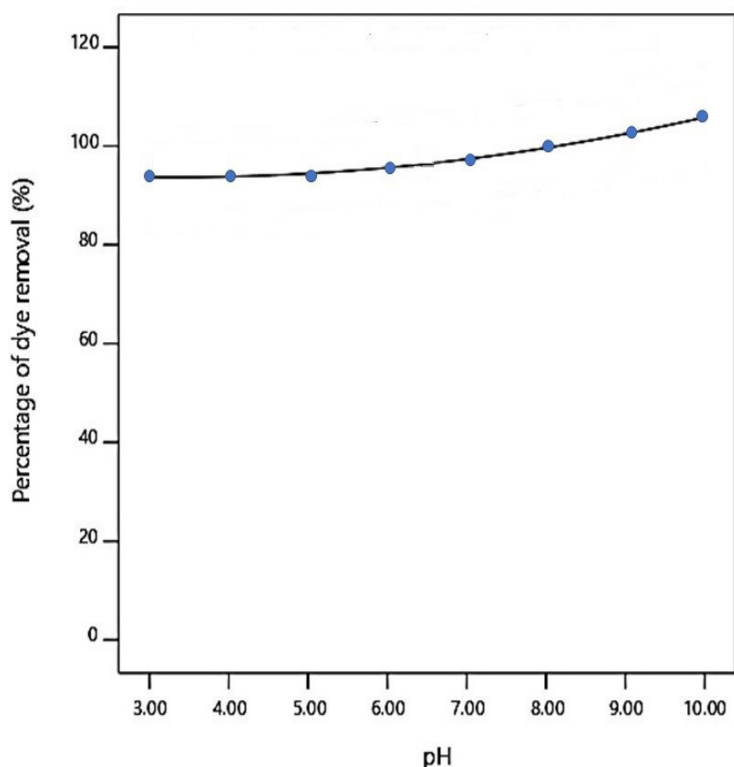


Figure 4. Percentage removal (%) of Rhodamine 6G by CS-NMAC in batch adsorption reaction at 27 °C, 150 rpm and 0.05 g CS-NMAC according to pH.

Equilibrium Adsorption Isotherm Studies

The performance and mechanism of dye removal were predicted and compared by fitting the experimental data into the corresponding linearized isotherm models (Figure 5). The respective parameters of each model are summarized in Table 2.

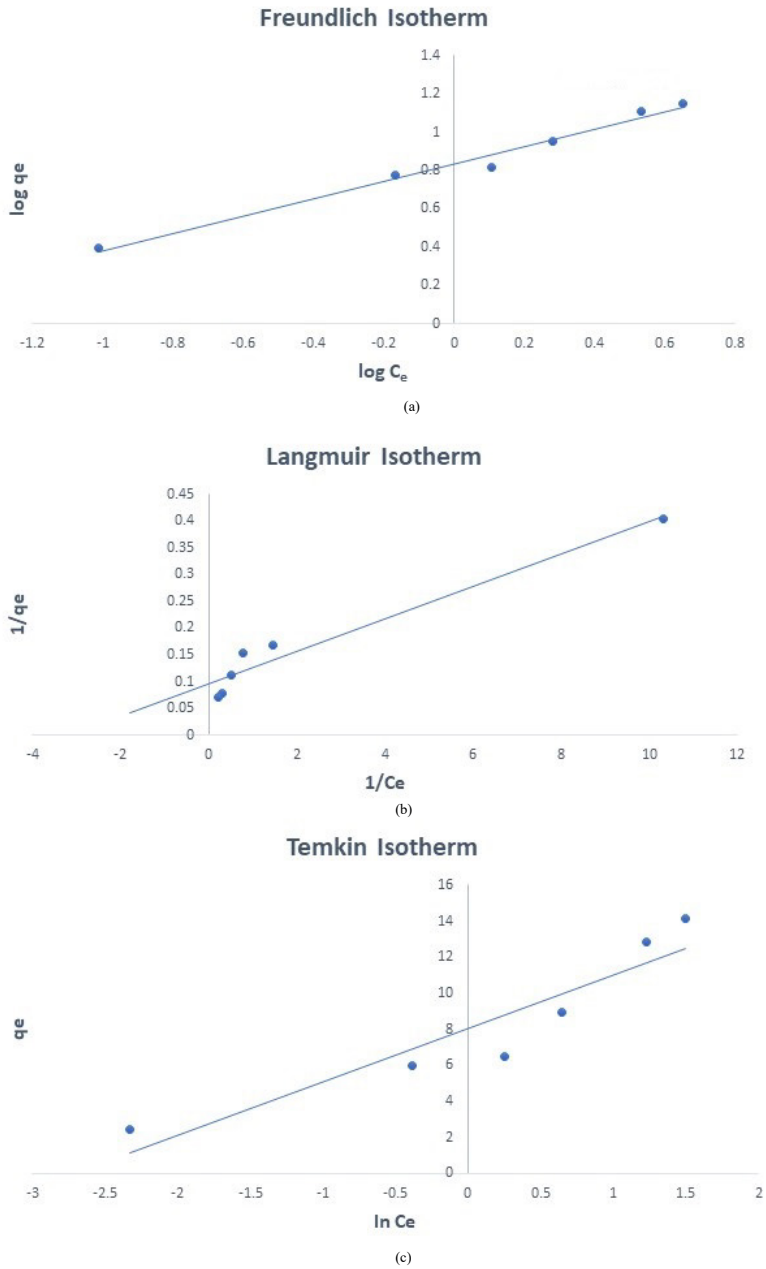


Figure 5. Graphs depicting the removal of Rhodamine 6G in aqueous solution by CS-NMAC at 27°C; 5, 10, 10, 15, 20 and 25 mg/L initial concentration (C_0); 0.05 g adsorbent dose; 150 rpm agitation rate; and 14.33 min contact time: (a) Langmuir isotherm, (b) Freundlich isotherm and (c) Temkin isotherm.

Table 2

Isotherm model parameters for Rhodamine 6G adsorption

Isotherm models	Parameters	Values
Freundlich	K_F	6.864
	n	2.208
	q_m (mg/g)	32.020
	R^2	0.981
Langmuir	K_L	0.3179
	R_L	0.0309–0.1367
	q_m (mg/g)	33.0033
	R^2	0.9514
Temkin	b (J/mol)	24.08
	K_T (L/g)	15.107
	R^2	0.8649

Among the isotherm models, the Freundlich model had the highest R^2 value of 0.981. The n value ($n = 2.208$) was sufficiently high for separation and indicating that Rhodamine 6G removal favoured the Freundlich isotherm model. An n value equals to one ($n = 1$) indicates that the partition between the adsorbent and the adsorbate is independent of concentration. However, when the n value greater unity ($n > 1$), the reaction has high affinity towards the occurrence of chemisorption between the adsorbate and the adsorbent; thus, it is considered chemisorption (Wang et al., 2015). This route reflects a multilayered adsorption process on a heterogeneous surface, which has the advantage of having more adjacent carbon atoms to provide interaction with adsorbing molecules. Similar findings were reported by Wannahari et al. (2018) and Mohammed et al. (2017) for the removal of heavy metals (Cu^{2+}). A comparison of the Rhodamine 6G adsorption performance among the other adsorbents in terms of adsorption capacity is shown in Table 3. The adsorption capacity of CS-NMAC was higher than that of the other adsorbents because of its high S_{BET} value, which indicated that CS-NMAC had a large surface area for adsorption.

Table 3

Comparison of the adsorption capacities of Rhodamine 6G with the adsorbents

Adsorbent	Adsorption capacity (mg/g)	Model	pH	S_{BET} (m^2/g)	References
Moroccan natural phosphate	6.84	Langmuir	5.2	18.8	Bensalah et al. (2017)

Table 3 (Continued)

Adsorbent	Adsorption capacity (mg/g)	Model	pH	SBET (m ² /g)	References
Kappa-carrageenan grafted with N-hydroxyethylacrylamide	8.38	Freundlich	>7	0.0502	Kulal and Badalamoole (2020)
Fe ₃ O ₄ -composited biochar derived from rice husk	9.42	Langmuir	7	Not cited	Suwunwong et al. (2020)
Mesoporous silica nanoparticles	13.70	Langmuir	Not cited	1078	Kachbouri et al. (2018)
Coconut shell-derived nanomagnetic adsorbent composite	32.02	Freundlich	7	1092.17	This study

Kinetic Models for the Adsorption of Rhodamine 6G Dye

The mechanism and potential rate-controlling step of Rhodamine 6G adsorption by CS-NMAC by applying adsorption kinetics models consisting of pseudo-first-order, pseudo-second order and intra-particle diffusion kinetic models. The obtained correlation coefficients (R^2) were used to assess the applicability of the kinetic models (Sharifi & Shoja, 2018). The values of the adsorption kinetic model constants are summarized in Table 4. The pseudo-second-order kinetic model showed an excellent correlation coefficient ($R^2 = 0.9995$) compared with the pseudo-first order and intra-particle diffusion models (Figure 6). Aside from high correlation value, the pseudo-second order showed high proximity between the experimental uptake capacity ($q_{e(\text{exp})}$) (14.445 mg/g) and the calculated uptake capacity ($q_{e(\text{cal})}$) (15.1515 mg/g), indicating that the adsorption of Rhodamine 6G to CS-NMAC was controlled by chemisorption. The presence of iron oxide nanoparticles endowed CS-NMAC with a strong ferromagnetic property. During the adsorption reaction, the Rhodamine 6G dye considerably faded, and the powdered CS-NMAC aggregated and homogeneously dispersed toward the external magnetic field. As a result, the strong ferromagnetic properties allowed for convenient separation and overcame the problem of remaining adsorbent residues. Valence forces were involved in the chemisorption process by sharing or exchanging electrons between the Rhodamine 6G dye molecules and the CS-NMAC surface (Figure 7).

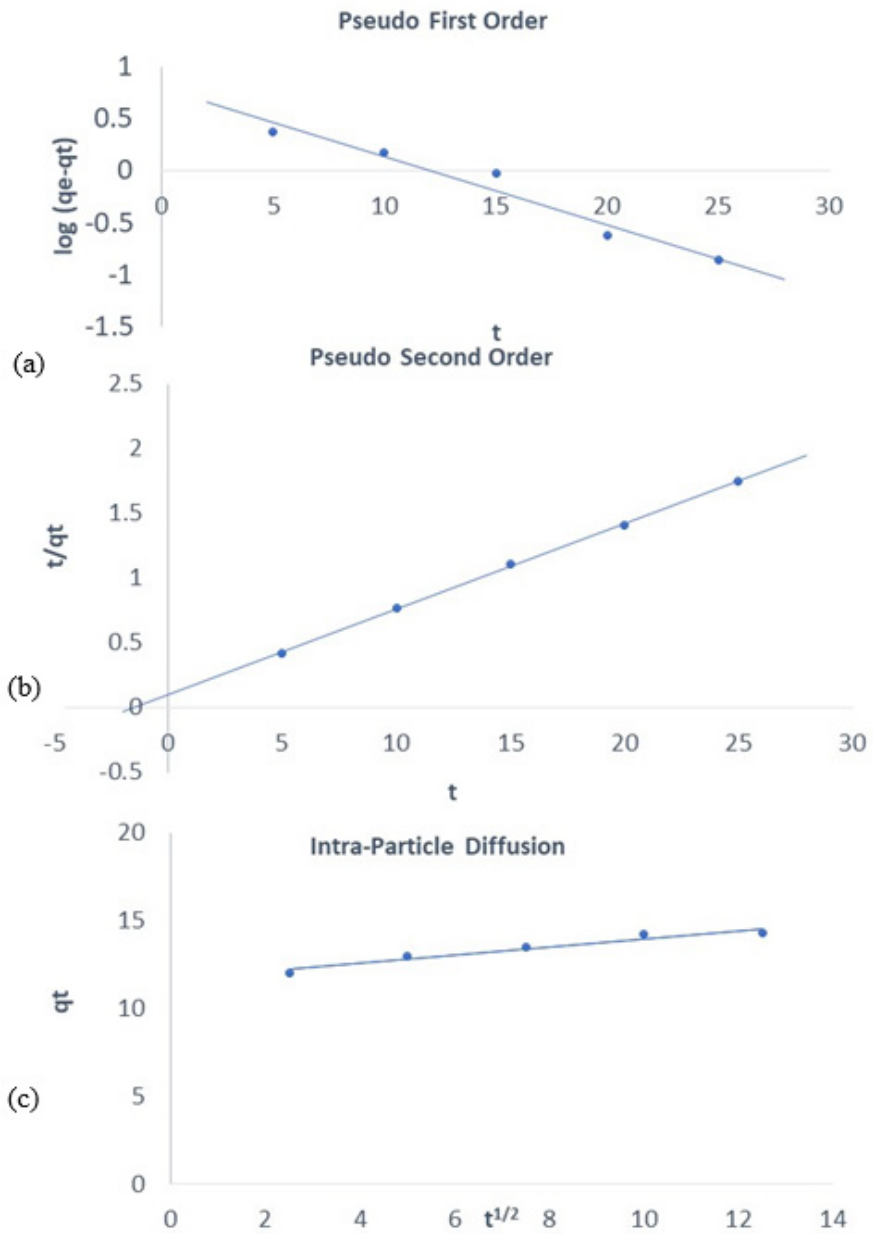


Figure 6. Representation of (a) pseudo-first order, (b) pseudo-second order and (c) intra- particle diffusion plots for Rhodamine 6G adsorption into CS-NMAC at 27 °C, 150 rpm agitation, 26.12 mg/L dye concentration and adsorbent dose of 0.05 g.

Table 4

Values of kinetic model constants for the adsorption of Rhodamine 6G

q_e (exp) (mg/g)	PSEUDO-FIRST ORDER			Pseudo-second order		
	q_e (cal) (mg/g)	k_1 (min ⁻¹)	R ²	q_e (cal) (mg/g)	k_2 (min ⁻¹)	R ²
14.4450	6.11223	0.1500	0.9572	15.1515	0.0437	0.9991

q_e (exp) (mg/g)	INTRAPARTICLE DIFFUSION		
	K_i (g/mg min ⁻¹)	C	R ²
14.4450	0.2296	11.6870	0.9469

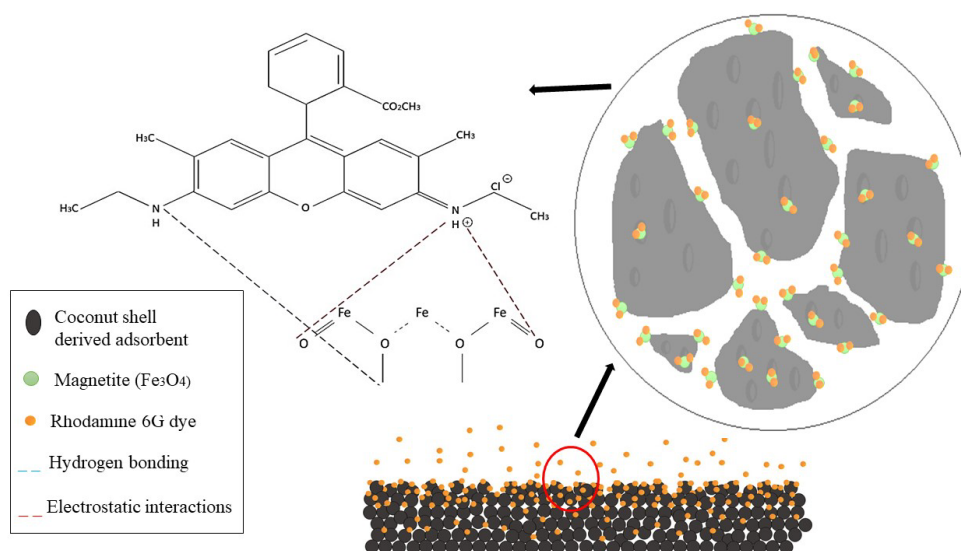


Figure 7. Chemisorption between Rhodamine 6G and surface of CS-NMAC

FTIR Analysis after Rhodamine 6G Adsorption into CS-NMAC

The peaks with respect to chemical functional groups observed before and after Rhodamine 6G dye adsorption are plotted in Figure 8. FTIR analysis was performed within 500–4000 cm⁻¹ to identify the functional groups on the surface of CS-NMAC that formed bonding structures during adsorption.

The peaks of CS-NMAC at 1716.07 cm^{-1} that appeared before adsorption and at 1718.53 cm^{-1} that appeared after adsorption were attributed to CN stretching. The peak at 1988.94 cm^{-1} corresponded to the C–H functional group before adsorption, but it shifted to 1845.52 cm^{-1} after adsorption. Prior to the adsorption reaction, asymmetric C=C stretching was observed at 1999.28 cm^{-1} , which later appeared at 1988.63 cm^{-1} after the reaction. The shift in CS-NMAC peaks during the adsorption reaction indicated interactions between the active sites on the surface of the adsorbent functional group and Rhodamine 6G (Sharifi & Shoja, 2018).

Moreover, the shift in O–H vibration peaks within $3522.17\text{--}3688.95\text{ cm}^{-1}$ before adsorption and the shift in O–H stretching peaks within $3503.76\text{--}3702.70\text{ cm}^{-1}$ after adsorption, as well as the shift in the peak intensity of Fe–O stretching from within $506.16\text{--}575.72\text{ cm}^{-1}$ to within $502.15\text{--}575.78\text{ cm}^{-1}$ after adsorption, affirmed the formation of hydrogen bonds. Popoola (2019) reported that the formation of hydrogen bonds during Cd^{2+} adsorption by nanomagnetic walnut shell rice husk was due to shifts in the peak of O–H.

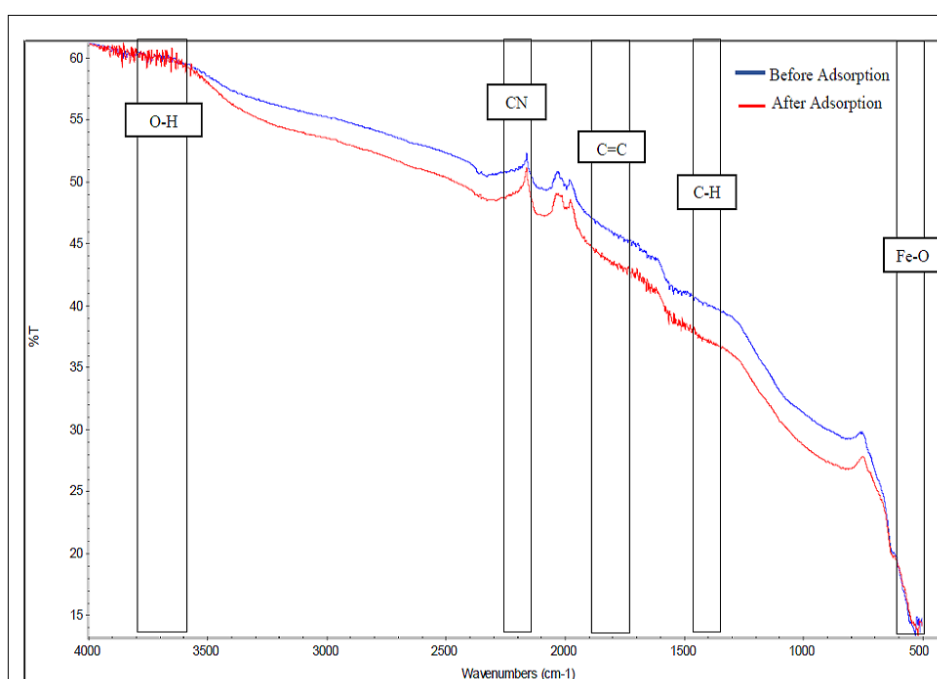


Figure 8. FTIR spectra of CS-NMAC before and after adsorption of Rhodamine 6G dye

Comparison of Removal Efficiency of CS-NMAC with that of CAC

The effectiveness of CS-NMAC in removing Rhodamine 6G from aqueous solution was evaluated via adsorption experiments by using CAC under the optimized conditions. CAC

was produced via steam activation ($\sim 1,000^{\circ}\text{C}$). The different methods for separating and removing Rhodamine 6G dye and the percentage of their removal are presented in Table 5.

Table 5

Percentage of Rhodamine 6G dye removal for each adsorption

Adsorbent	Separation Method	Percentage of Dye Removal (%)	Uptake Capacity q (mg/g)
CS-NMAC	Magnet + Filtration	99.9968	31.219
CAC	Filtration	99.9964	28.029

CAC and the nanomagnetic biocarbon composite both exhibited good adsorption capacity and achieved high removal efficiency (Table 5). Both displayed high percentage ($\sim 99\%$) of Rhodamine 6G dye removal; thus, they were effective adsorbents. The adsorption capacity of CS-NMAC (nonsteam activated) was also high and comparable to that of steam-activated CAC because of the availability and higher affinity of nanomagnetic particles. The presence and characteristics of nanoparticles affected the adsorption capacity of the adsorbents.

Moreover, CS-NMAC held a competitive advantage over CAC in terms of diamagnetic properties. Nanomagnetic biocarbon composites that resulted from the modification and innovation of biocarbon could be easily separated from the solution and thus resolve the separation problem of CAC. Furthermore, CS-NMAC could adsorb various pollutants, such as cationic dye (Rhodamine 6G, this study) and heavy metals (Cr^{2+}) (Wannahari et al., 2018) because of the amphoteric properties of magnetite (Fe_3O_4) on the surface of the adsorbent.

CONCLUSION

CS-NMAC was found to have a high active area for adsorption as indicated by S_{BET} ($1092.17 \text{ m}^2/\text{g}$) and PVT ($0.6715 \text{ cm}^3/\text{g}$). Both characteristics are advantageous for surface-bound adsorption processes. The presence of maghemite, hematite and wuestite as confirmed by XRD analysis indicated that nanosized iron oxide particles were embedded on the matrix of the CS-NMAC surface. FTIR analysis revealed that the FeO functional group on the surface of CS-NMAC was vital to the adsorption and separation in solution. The best fit model for CS-NMAC adsorption was found to be the Freundlich model ($R^2 = 0.981$), which revealed that adsorption occurred on the heterogeneous surface with a maximum adsorption capacity of 32.020 mg/g . However, Rhodamine 6G adsorption obeyed the pseudo-second-order reaction, implying the onset of chemisorption in the process. This

situation likely occurred owing to the valence electron of surface atoms of maghemite, hematite and wuestite crystals. Furthermore, the dye removal performance was comparable to that of CAC but with a more convenient magnetic separation of the used material from the solution. Therefore, iron oxide nanoparticles on the surface of CS-NMAC not only greatly influenced the performance in adsorption but also enhanced the isotherm and kinetics of the adsorbent.

ACKNOWLEDGEMENT

The authors acknowledge the financial support from Universiti Malaysia Kelantan (R/SGJP/A07.00/01397A/005/2018/00570).

REFERENCES

- Ahmadgurabi, N. G., Koochi, A. D., & Pirbazari, A. E. (2018). Fabrication, characterization regeneration and application of nanomagnetic Fe_3O_4 @ fish scale as a bio-adsorbent for removal of methylene blue. *Journal of Water and Environmental Nanotechnology*, 3(3), 219-234. <https://doi.org/10.22090/jwent.2018.03.003>
- Azlan, A., & Haseeb, M. (2019). Radio frequency identification (RFID) technology as a strategic tool towards higher performance of supply chain operations in textile and apparel industry of Malaysia. *Uncertain Supply Chain Management*, 7(2), 215-226. <https://doi.org/10.5267/j.uscm.2018.10.004>
- Bahrami, A., Soltani, N., Pech-Canul, M. I., & Gutierrez, C. A. (2016). Development of metal-matrix composites from industrial/agricultural waste materials and their derivatives. *Critical Reviews in Environmental Science and Technology*, 46(2), 143-208. <http://dx.doi.org/10.1080/10643389.2015.1077067>
- Bensalah, H., Bekheet, M. F., Alami, S., & Ouammou, M. (2017). Removal of cationic and anionic textile dyes with Moroccan natural phosphate. *Journal of Environmental Chemical Engineering*, 5(3), 2189-2199. <https://doi.org/10.1016/j.jece.2017.04.021>
- Bishnoi, S., Kumar, A., & Selvaraj, R. (2017). Facile synthesis of magnetic iron oxide nanoparticles using inedible *Cynometra ramiflora* fruit extract waste and their photocatalytic degradation of methylene blue dye. *Materials Research Bulletin*, 97, 121-127. <https://doi.org/10.1016/j.materresbull.2017.08.040>
- Booker, N. A., Keir, D., Priestley, A. J., Ritchie, C. B., Sudarmana, D. L., & Woods, M. A. (1991). Sewage clarification with magnetite particles. *Water Science & Technology*, 23, 1703-1712.
- Feng, Z., Chen, H., Li, H., Yuan, R., Wang, F., Chen, Z., & Zhou, B. (2020). Preparation, characterization, and application of magnetic activated carbon for treatment of biologically treated papermaking wastewater. *Science of The Total Environment*, 713, Article 136423. <https://doi.org/10.1016/j.scitotenv.2019.136423>
- Feng, Z., Yuan, R., Wang, F., Chen, Z., Zhou, B., & Chen, H. (2021). Preparation of magnetic biochar and its application in catalytic degradation of organic pollutants: A review. *Science of The Total Environment*, 765, Article 142673. <https://doi.org/10.1016/j.scitotenv.2020.142673>
- Godwin, P. M., Pan, Y., Xiao, H., & Afzal, M. T. (2019). Progress in preparation and application of modified biochar for improving heavy metal ion removal from wastewater. *Journal of Bioresources and Bioproducts*, 4(1), 31-42. <https://doi.org/10.21967/jbb.v4i1.180>

- Guo, Z., Chen, R., Yang, R., Yang, F., Chen, J., Li, Y., Zhou, R., & Xu, J. (2020). Science of the total environment synthesis of amino-functionalized biochar / spinel ferrite magnetic composites for low-cost and efficient elimination of Ni (II) from wastewater. *Science of the Total Environment*, 722, Article1 37822. <https://doi.org/10.1016/j.scitotenv.2020.137822>
- Hao, Z., Wang, C., Yan, Z., Jiang, H., & Xu, H. (2018). Magnetic particles modification of coconut shell-derived activated carbon and biochar for effective removal of phanol from water. *Chemosphere*, 211, 962-969. <https://doi.org/10.1016/j.chemosphere.2018.08.038>
- Intachai, S., Pimchan, P., & Sumanatrakul, P. (2019). Synthesis of NiAl - layered double oxide as inorganic adsorbent for eliminating dye from solution. *Naresuan University Journal: Science and Technology*, 4(27), 66-74. <https://doi.org/10.14456/nujst.2019.37>
- Jasmin, S., Jan, M. R., Haq, A., & Khan, Y. (2013). Removal of rhodamine B from aqueous solutions and wastewater by walnut shells: Kinetics, equilibrium and thermodynamics studies. *Frontiers of Chemical Science and Engineering*, 7(4), 428-436. <https://doi.org/10.1007/s11705-013-1358-x>
- Kachbouri, S., Mnasri, N., Elaloui, E., & Moussaoui, Y. (2018). Tuning particle morphology of mesoporous silica nanoparticles for adsorption of dyes from aqueous solution. *Journal of Saudi Chemical Society*, 22(4), 405-415. <https://doi.org/10.1016/j.jscs.2017.08.005>
- Kandpal, N. D., Sah, N., Loshali, R., Joshi, R., & Prasad, J. (2014). Co-precipitation method of synthesis and characterization of iron oxide nanoparticles. *Journal of Scientific & Industrial Research*, 73, 87-90.
- Khan, Z. H., Gao, M., Qiu, W., Islam, S., & Song, Z. (2020). Mechanisms for cadmium adsorption by magnetic biochar composites in an aqueous solution. *Chemosphere*, 246, Article 125701. <https://doi.org/10.1016/j.chemosphere.2019.125701>
- Kong, X., Liu, Y., Pi, J., Li, W., & Liao, Q. (2017). Low-cost magnetic herbal biochar: Characterization and application for antibiotic removal. *Environmental Science and Pollution Research*, 24, 6679-6687. <https://doi.org/10.1007/s11356-017-8376-z>
- Kuang, Y., Zhang, X., & Zhou, S. (2020). Adsorption of methylene blue in water onto activated carbon by surfactant modification. *Water*, 12(587), 1-19. <https://doi.org/doi:10.3390/w12020587>
- Kulal, P., & Badalamoole, V. (2020). Hybrid nanocomposite of kappa-carrageenan and magnetite as adsorbent material for water purification. *International Journal of Biological Macromolecules*, 165, 542-553. <https://doi.org/10.1016/j.ijbiomac.2020.09.202>
- Li, C., Gao, Y., Li, A., Zhang, L., Ji, G., Zhu, K., & Wang, X. (2019). Synergistic effects of anionic surfactants on adsorption of norfloxacin by magnetic biochar derived from furfural residue. *Environmental Pollution*, 254, 1-8. <https://doi.org/10.1016/j.envpol.2019.113005>
- Mane, V. S., & Babu, P. V. V. (2011). Studies on the adsorption of brilliant green dye from aqueous solution onto low-cost NaOH treated saw dust. *Desalination*, 273(2-3), 321-329. <https://doi.org/10.1016/j.desal.2011.01.049>
- Miranda, A., Serrão, N. O., Celestino, G. D. G., Takeno, M. L., Tiago, N., Antunes, B., Stefan, I., Lizandro, M., & Freitas, F. A. D. (2019). Removal of rhodamine 6G from synthetic effluents using *Clitoria fairchildiana* pods as low-cost biosorbent. *Environmental Science and Pollution Research*, 27, 2868-2880. <https://doi.org/10.1007/s11356-019-07114-6>

- Mohammed, M. A., Abubakar, B. I. & Kurna, B. B. (2017). Equilibrium and kinetics studies of adsorption of safranin-O from aqueous solutions using pineapple peels. *Arid Zone Journal of Engineering, Technology and Environment*, 13(6), 671-687.
- Muzarpar, M. S., Leman, A. M., Rahman, K. A., Shayfull, Z., & Irfan, A. R. (2020). Exploration sustainable base material for activated carbon production using agriculture waste as raw materials: A review exploration sustainable base material for activated carbon production using agriculture waste as raw materials: A review. In *IOP Conference Series: Materials Science and Engineering* (Vol. 864, No. 1, p. 012022). IOP Publishing. <https://doi.org/10.1088/1757-899X/864/1/012022>
- Nadzri, S. N. I. H. A., Sultan, M. T. H., Shah, A. U. M., Safri, S. N. A., Talib, A. R. A., Jawaid, M., & Basri, A. A. (2020). A comprehensive review of coconut shell powder composites: Preparation, processing, and characterization. *Journal of Thermoplastic Composite Materials*, 1-24. <https://doi.org/10.1177/0892705720930808>
- Nimibofa, A., Augustus, N. E., & Donbebe, W. (2017). Modelling and interpretation of adsorption isotherms. *Journal of Chemistry*, 2017, 1-11. <https://doi.org/10.1088/1757-899X/864/1/012022>
- Patrick, E., Ebere, M., & Echegi, U. S. (2014). Effect of process factors on the adsorption of MB dye using *Adenia lobata* Fiber. *International Journal of Innovative Research in Science, Engineering and Technology*, 3(10). <https://doi.org/10.15680/IJRSET.2014.0310004>
- Popoola, L. T. (2019). Nano-magnetic walnut shell-rice husk for Cd (II) sorption: Design and optimization using artificial intelligence and design expert. *Heliyon*, 5(8), Article e02381. <https://doi.org/10.1016/j.heliyon.2019.e02381>
- Rasheed, T., & Bilal, M. (2017). Reaction mechanism and degradation pathway of rhodamine 6G by photocatalytic treatment. *Water Air Soil Pollution*, 228(291), 1-10. <https://doi.org/10.1007/s11270-017-3458-6>
- Reguyal, F., & Sarmah, A. K. (2018). Adsorption of sulfamethoxazole by magnetic biochar: Effects of pH, ionic strength, natural organic matter and 17 α -ethinylestradiol. *Science of the Total Environment*, 628, 722-730. <https://doi.org/10.1016/j.scitotenv.2018.01.323>
- Sahu, O., & Singh, N. (2019). Significance of bioadsorption process on textile industry wastewater. In *The impact and prospects of green chemistry for textile technology* (pp. 367-416). Woodhead Publishing. <https://doi.org/10.1016/B978-0-08-102491-1.00013-7>
- Sannasi, P., Awang, H., & Barasarathi, J. (2021). Synthesis of magnetic activated carbon treated with sodium dodecyl sulphate. *Pertanika Journal of Science and Technology*, 29(1), 427-444. <https://doi.org/10.47836/pjst.29.1.24>
- Santhi, M., & Kumar, P. E. (2015). Adsorption of rhodamine B from an aqueous solution: Kinetic, equilibrium and thermodynamic studies. *International Journal of Innovative Research in Science, Engineering and Technology*, 4(2), 497-510. <https://doi.org/10.1016/B978-0-08-102491-1.00013-7>
- Sharifi, S. H., & Shoja, H. (2018). Optimization of process variables by response surface methodology for methylene blue dye removal using spruce sawdust/Mgo nano-biocomposite. *Journal of Water Environment Nanotechnology*, 3(2), 157-172. <https://doi.org/10.22090/JWENT.2018.02.007>

- Sundarajoo, A., & Maniyam, M. N. (2019). Enhanced decolourization of congo red dye by Malaysian rhodococcus UCC 0010 immobilized in calcium alginate. *Journal of Advanced Research Design*, 62(1), 1-9.
- Suwunwong, T., Patho, P., Choto, P., & Phoungthong, K. (2020). Enhancement the rhodamine 6G adsorption property on Fe₃O₄ -composited biochar derived from rice husk. *Materials Research Express*, 7, Article 025511. <https://doi.org/10.1088/2053-1591/ab6b58>
- Vijayakumar, G., Tamilarasan, R., & Dharmendirakumar, M. (2012). Adsorption, kinetics, equilibrium and thermodynamic studies on the removal of basic dye rhodamine-B from aqueous solution by the use of natural adsorbent perlite. *Journal of Materials and Environmental Science*, 3(1), 157-170. <https://doi.org/10.1016/j.arabjc.2016.11.009>
- Vyavahare, G., Jadhav, P., Jadhav, J., Patil, R., Aware, C., Patil, D., Gophane, A., Yang, Y. H., & Gurav, R. (2019). Strategies for crystal violet dye sorption on biochar derived from mango leaves and evaluation of residual dye toxicity. *Journal of Cleaner Production*, 207, 296-305. <https://doi.org/10.1016/j.jclepro.2018.09.193>
- Wang, J., & Kaskel, S. (2012). KOH activation of carbon-based materials for energy storage. *Journal of Material Chemistry*, 22(45), 23710-23725. <https://doi.org/10.1039/C2JM34066F>
- Wang, J., Liu, G., Li, T., & Zhou, C. (2015). Physicochemical studies toward the removal of Zn(ii) and Pb(ii) ions through adsorption on montmorillonite-supported zero-valent iron nanoparticles. *RSC Advances*, 5(38), 29859-29871. <https://doi.org/10.1039/C5RA02108A>
- Wannahari, R., Sannasi, P., Nordin, M. F. M., & Mukhtar, H. (2018). Sugarcane bagasse derived nano magnetic adsorbent composite (SCB-NMAC) for removal of Cu²⁺ from aqueous solution. *ARP Journal of Engineering and Applied Sciences*, 13(1), 1-9.
- Wimalawansa, S. J. (2013). Purification of contaminated water with reverse osmosis: effective solution of providing clean water for human needs in developing countries. *International Journal of Emerging Technology and Advanced Engineering*, 3(12), 75-89.